

Article

Unfolding of Helical Poly(*L*-Glutamic Acid) in *N,N*-Dimethylformamide Probed by Pyrene Excimer Fluorescence (PEF)

Weize Yuan, Remi Casier and Jean Duhamel * 

Institute for Polymer Research, Waterloo Institute of Nanotechnology, Department of Chemistry, University of Waterloo, Waterloo, ON N2L 3G1, Canada; w96yuan@mit.edu (W.Y.); remi.casier@uwaterloo.ca (R.C.)

* Correspondence: jduhamel@uwaterloo.ca; Tel.: +1-519-888-4567 (ext. 35916)

Abstract: The denaturation undergone by α -helical poly(*L*-glutamic acid) (PLGA) in *N,N*-dimethylformamide upon addition of guanidine hydrochloride (GdHCl) was characterized by comparing the fluorescence of a series of PLGA constructs randomly labeled with the dye pyrene (Py-PLGA) to that of a series of Py-PDLGA samples prepared from a racemic mixture of *D,L*-glutamic acid. The process of pyrene excimer formation (PEF) was taken advantage of to probe changes in the conformation of α -helical Py-PLGA. Fluorescence Blob Model (FBM) analysis of the fluorescence decays of the Py-PLGA and Py-PDLGA constructs yielded the average number ($\langle N_{\text{blob}} \rangle$) of glutamic acids located inside a *blob*, which represented the volume probed by an excited pyrenyl label. $\langle N_{\text{blob}} \rangle$ remained constant for randomly coiled Py-PDLGA but decreased from ~ 20 to ~ 10 glutamic acids for the Py-PLGA samples as GdHCl was added to the solution. The decrease in $\langle N_{\text{blob}} \rangle$ reflected the decrease in the local density of PLGA as the α -helix unraveled in solution. The changes in $\langle N_{\text{blob}} \rangle$ with GdHCl concentration was used to determine the change in Gibbs energy required to denature the PLGA α -helix in DMF. The relationship between $\langle N_{\text{blob}} \rangle$ and the local density of macromolecules can now be applied to characterize the conformation of macromolecules in solution.

Keywords: poly(glutamic acid); pyrene excimer fluorescence; fluorescence blob model; denaturation



Citation: Yuan, W.; Casier, R.; Duhamel, J. Unfolding of Helical Poly(*L*-Glutamic Acid) in *N,N*-Dimethylformamide Probed by Pyrene Excimer Fluorescence (PEF). *Polymers* **2021**, *13*, 1690. <https://doi.org/10.3390/polym13111690>

Academic Editor: José Manuel Gaspar Martinho

Received: 19 April 2021
Accepted: 18 May 2021
Published: 22 May 2021

Publisher's Note: MDPI stays neutral with regard to jurisdictional claims in published maps and institutional affiliations.



Copyright: © 2021 by the authors. Licensee MDPI, Basel, Switzerland. This article is an open access article distributed under the terms and conditions of the Creative Commons Attribution (CC BY) license (<https://creativecommons.org/licenses/by/4.0/>).

1. Introduction

The Fluorescence Blob Model (FBM) was introduced in 1999 as a mathematical tool to extract quantitative information about the internal dynamics of polymers, that had been randomly labeled with the fluorescent dye pyrene [1]. As discussed in several reviews [2–5], the FBM takes advantage of the ability of an excited pyrene to form an excimer upon diffusive encounter with a ground-state pyrene inside the volume probed by the excited pyrene, and referred to as a *blob*. In turn, the *blob* could be used as a unit volume to divide the polymer coil into a cluster of identical subvolumes. Random labeling of a polymer with a pyrene derivative ensured that the pyrenyl labels would distribute themselves randomly among the *blobs* according to a Poisson distribution. Analysis of the fluorescence decays acquired with solutions of the pyrene-labeled polymers yielded the average number ($\langle n \rangle$) of ground-state pyrenes per *blob*, which could be related to the number (N_{blob}) of structural units encompassed inside a *blob*. For different polymers, a larger N_{blob} typically indicated that the excited pyrenyl label could probe a larger volume, reflecting a more flexible polymeric backbone.

While these early studies [1–5] established the FBM as an interesting means for gauging the flexibility of one polymer backbone against another, they overlooked an important aspect of the FBM, which is its ability to provide quantitative information about the local density of a macromolecule. In turn, this information could be related to the conformation of the macromolecule of interest, a most important research topic in macromolecular

science. Based on this insight, a combination of pyrene excimer formation (PEF), FBM, and molecular mechanics optimizations (MMOs) was applied to yield the internal density of arborescent poly(*L*-glutamic acid)s (PLGAs) [6], confirm the helical conformation of amylose in dimethylsulfoxide (DMSO) [7], PLGA in *N,N*-dimethylformamide (DMF) [8–10], and poly(*L*-lysine) in acetonitrile/water mixtures [11], predict the 3_{10} -helical conformation of PLGA in DMSO [12], introduce the Solution-Cluster model to describe the interior of amylopectin in DMSO [13,14], and provide the first 1:1 direct relationship between the experimental and predicted folding time of proteins [15,16].

The ability to characterize the conformation of macromolecules in solution makes N_{blob} a central parameter in the study of macromolecules by PEF [1–5], in the same manner as the radius of gyration (R_g) and ellipticity (θ) are central parameters to, respectively, scattering [17–19] or circular dichroism (CD) [20–26] measurements to probe the conformation of, respectively, synthetic macromolecules or proteins in solution. To further assess the ability of N_{blob} to probe macromolecular conformations in solution, the present study investigates how N_{blob} reports on the unravelling of an α -helical PLGA in DMF as guanidine hydrochloride (GdHCl), a well-known denaturing agent [27], is added to the solution. To this end, a sample of PLGA and of poly(*D,L*-glutamic acid) (PDLGA) were randomly labeled with 1-pyrenemethylamine (PyMA) to yield Py-PLGA and Py-PDLGA, respectively, and PEF was applied to probe conformational changes in PLGA as GdHCl was added to the solution. PLGA is known to adopt an α -helical conformation in DMF [8–10], while the racemic nature of PDLGA imposes that it adopts a random coil conformation under any solvent condition. Consequently, PDLGA with its random coil conformation regardless of solvent conditions provided an ideal baseline against which the conformation of PLGA could be compared as GdHCl was added to the polypeptide solutions. The fluorescence decays of dilute solutions of Py-PLGA and Py-PDLGA in DMF were acquired and analyzed according to the FBM to retrieve N_{blob} as a function of the concentration of GdHCl added to the solutions. Comparison of the N_{blob} values obtained for the randomly coiled Py-PDLGA samples and the α -helical Py-PLGA samples in DMF without GdHCl provided a means to assess the extent of denaturation in the PLGA α -helix as GdHCl was added.

The results show that N_{blob} reflected the extent of the denaturation of the PLGA α -helix, decreasing as the helix unfolded with increasing GdHCl concentration, while N_{blob} remained constant for PDLGA in DMF over the entire GdHCl concentration range. The N_{blob} value was also employed to determine the molar fraction of native (f_N) and denatured (f_D) PLGA molecules in solution. In turn, the f_N and f_D fractions could be applied to determine the equilibrium constant (K^{unfold}) for the Native \rightleftharpoons Denatured equilibrium at each GdHCl concentration [28,29] and yield the change in Gibbs energy ($\Delta_{\text{unfold}}G(\text{DMF})$) for the unfolding of the α -helical PLGA in DMF in the same manner, that experiments using CD or LS would do. In summary, these PEF experiments further support the notion that N_{blob} , determined for macromolecules randomly labeled with pyrene, reports on the local density of macromolecules and can be used to infer their conformation in solution.

2. Materials and Methods

2.1. Sample Preparation

The preparation of the Py-PLGA and Py-PDLGA samples has been described earlier [10]. Six Py-PLGA samples and five Py-PDLGA samples were used in these experiments. Their chemical structure is described in Figure 1. The samples were dissolved in DMF (Sigma, $\geq 99.8\%$) before being diluted so that their concentration in pyrenyl label would equal 2.5×10^{-6} M, low enough to avoid any intermolecular interactions. Oxygen dissolved in the Py-PLGA solutions was outgassed by passing a gentle flow of 99.99% high purity N_2 (Praxair, N4.0) for 30 min. Steady-state (SSF) and time-resolved (TRF) fluorescence experiments (SSF: LS-100 Photon Technology International, London, ON, Canada; TRF: IBH Ltd, Glasgow, Scotland, UK) were conducted with the degassed solutions.

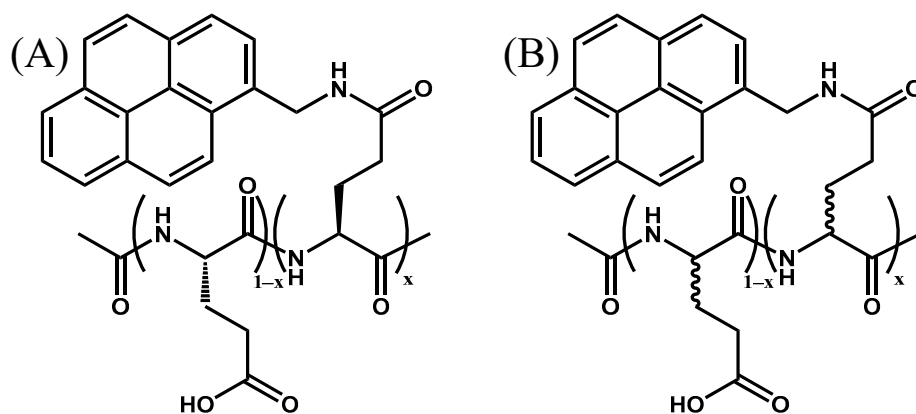


Figure 1. Chemical structure of (A) Py(x)-PLGA ($x = 2.9, 4.4, 4.9, 6.9, 9.0,$ and 14.3 mol%) and (B) Py(x)-PDLGA ($x = 6.0, 8.0, 10.4, 11.3,$ and 12.3 mol%) samples used in this study.

2.2. Steady-State Fluorescence

A PTI spectrofluorometer was used to acquire the SSF spectra with a 344 nm excitation wavelength. The excitation and emission slit widths were set at 2 and 1 nm, respectively. The SSF spectrum was then analyzed by determining the fluorescence intensity of the monomer (I_M) and excimer (I_E) from the integration of the area under the spectrum from 372 to 378 nm and from 500 to 530 nm, respectively. These intensities were used to determine the I_E/I_M ratio, which was employed to gauge the PEF efficiency.

2.3. Time-Resolved Fluorescence

The TRF decays were acquired with an IBH time-correlated single photon counting (TC-SPC) fluorometer using a 340 nm-NanoLED for excitation. The solutions were excited at 344 nm with an excitation monochromator and the monomer and excimer fluorescence decays were collected at 375 and 510 nm using a 370 and 495 nm cutoff filter, respectively. A repetition rate of 1 MHz or 500 kHz, time per channel of 1.02 or 2.04 ns/ch, and number of counts at the decay maximum of 40,000 or 20,000 counts were applied to the monomer and excimer fluorescence decays, respectively. These experimental settings were the same as those reported in earlier publications [10,12].

2.4. Fluorescence Decay Analysis

The FBM was employed to fit the TRF decays [1–5] using in-house software. The FBM assumes that five different pyrene species exist in solution. The species Py_{diff}^* represents the excited pyrenes, that diffuse toward a ground-state pyrene to yield the species $Py_{k_2}^*$, where the excited and the ground-state pyrene labels are close enough to rearrange rapidly with a large rate constant k_2 to form an excimer. The pyrenes, that result in excimer formation, are referred to as $E0^*$ or D^* depending on whether the excimers produced are the result of the interaction between two well-stacked or two poorly stacked pyrenes, respectively. The fifth species, Py_{free}^* cannot form excimer and emits as if it were free in solution. The natural lifetime of the three species Py_{diff}^* , $Py_{k_2}^*$, and Py_{free}^* is that of the pyrene monomer (τ_M), whereas $E0^*$ and D^* emit with their natural lifetimes τ_{E0} and τ_D , respectively. The monomer and excimer fluorescence decays were fitted globally first with the program globmis90lbg, where k_2 is allowed to float freely, and then with the program globmis90obg, where k_2 is fixed in the analysis to its average value obtained with the earlier round of fits. The analysis provides the molar fractions f_{diff} , f_{k_2} , f_{free} , f_{E0} , and f_D of the pyrene species Py_{diff}^* , $Py_{k_2}^*$, Py_{free}^* , $E0^*$, and D^* , respectively. The sum of the fractions f_{E0} and f_D is referred to as f_{agg} since it represents the molar fraction of aggregated pyrenes. The FBM analysis also yields the average number $\langle n \rangle$ of ground-state pyrenes inside a *blob*, the product $k_e \times [blob]$ of the rate constant k_e for the exchange of ground-state pyrenes between *blobs* and the *blob* concentration $[blob]$, and the rate constant k_{blob} for diffusive encounters between two pyrenyl labels inside a *blob*. All the parameters retrieved

from the fit of the fluorescence decays were optimized with the Marquardt–Levenberg algorithm [30]. The equations used to fit the monomer and excimer fluorescence decays globally according to the FBM are provided as Supplementary Material (SM) as Equations (S1) and (S2), respectively, along with tables listing the FBM parameters retrieved from this analysis. In turn, the number of structural units found inside the volume of a *blob* (N_{blob}) can be obtained from $\langle n \rangle$ according to Equation (1), where x is the molar fraction of glutamic acids, that were labeled with 1-pyrenmethylamine (see Figure 1), and $f_{M\text{free}}$ represents the molar fraction of the Py_{free}^* species contributing to the monomer decay.

$$N_{\text{blob}} = \frac{\langle n \rangle}{x} (1 - f_{M\text{free}}) \quad (1)$$

3. Results

3.1. Steady-State Fluorescence

Since Py-PLGA adopts an α -helical conformation in DMF [8–10,31], the effect of GdHCl (Sigma, $\geq 99\%$), a well-known denaturing agent [27], on the denaturation of the PLGA helix was investigated by monitoring the fluorescence response of the Py-PLGA constructs as a function of the GdHCl concentration, which was varied from 0.1 to 5 M. The SSF spectra of solutions in DMF of five Py-PLGA and five Py-PDLGA samples were acquired for different GdHCl concentrations. The effect of the addition of GdHCl to the solution of Py(14.0)-PLGA and Py(10.4)-PDLGA in DMF is shown in Figure 2A,B after normalization at 375 nm, which corresponds to the 0–0 transition of pyrene. For both samples, the fluorescence of the pyrene excimer centered at 480 nm decreased with increasing GdHCl concentration. Although this effect was observed for all Py-PGA samples, it was more pronounced for the Py-PLGA samples. This is illustrated in a more quantitative manner by plotting the I_E/I_M ratio as a function of [GdHCl] in Figure 2C,D.

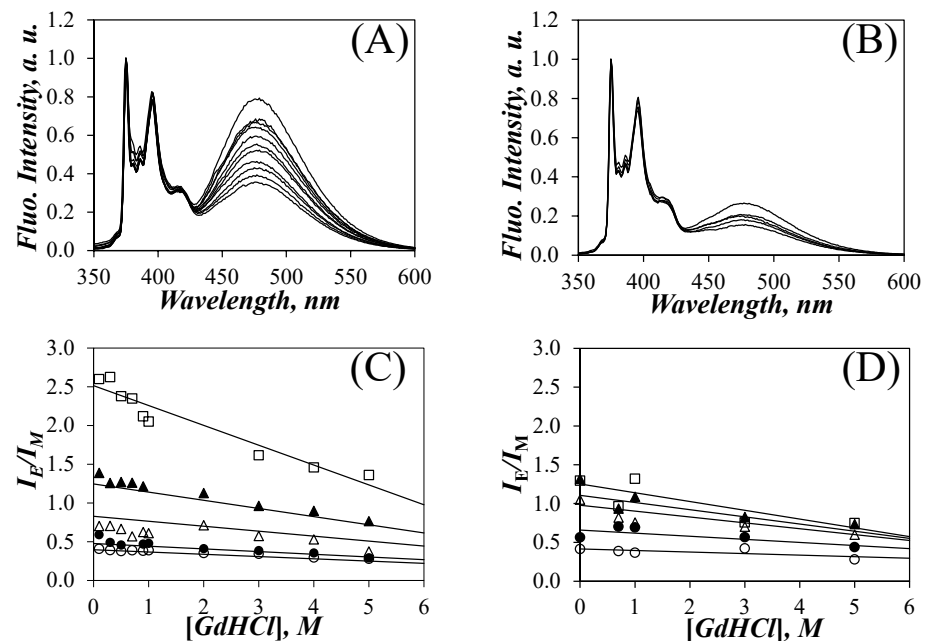


Figure 2. SSF spectra of (A) Py(14.0)-PLGA and (B) Py(10.4)-PDLGA in DMF with different GdHCl concentrations. From bottom to top: (A) [GdHCl] = 5.0, 4.0, 3.0, 2.0, 1.0, 0.9, 0.7, 0.5, 0.3, 0.1, 0.0 M and (B) [GdHCl] = 5.0, 3.0, 1.0, 0.7, and 0.0 M. Plots of I_E/I_M for (C) Py(x)-PLGA, where x = (○) 4.4, (●) 4.9, (△) 6.9, (▲) 9.0, and (□) 14.3 mol%, and (D) Py(x)-PDLGA, where x = (○) 6.0, (●) 8.0, (△) 10.4, (▲) 11.3, and (□) 12.3 mol%.

The behavior of the I_E/I_M ratio could be discussed in terms of Equation (2) [32], which shows how the I_E/I_M ratio is related to the rate constant k_{diff} of diffusive encounters

between an excited and a ground-state pyrenyl label and the local pyrene concentration $[Py]_{loc}$. As described by Equation (2), the reduction in I_E/I_M could be a result of one or more of the following three effects. First, the increase in viscosity by the addition of GdHCl is expected to reduce k_{diff} . Second, the probability of PEF upon encounter between an excited and a ground-state pyrenyl label [33] might change with GdHCl concentration and is known to affect k_{diff} . Third, the denaturation of the PLGA α -helix, which would reduce $[Py]_{loc}$. The difficulty in identifying which one of these parameters best rationalized the effects observed with the I_E/I_M ratios was resolved by applying the FBM analysis to the decays acquired with the pyrene-labeled samples. As a matter of fact, the FBM is designed to separate the contributions arising from k_{diff} and $[Py]_{loc}$ with the parameters $k_{blob} (=k_{diff} \times (1/V_{blob}))$, where V_{blob} is the *blob* volume and $1/V_{blob}$ represents the concentration equivalent to one ground-state pyrene inside a *blob* and $\langle n \rangle (= [Py]_{loc} \times V_{blob})$. $\langle n \rangle$ can then be used to determine the number N_{blob} of GA's contained within each blob volume according to Equation (1) [1–5].

$$\frac{I_E}{I_M} \propto k_{diff} \times [Py]_{loc} \quad (2)$$

3.2. Time-Resolved Fluorescence

The fluorescence decays of the pyrene monomer and excimer were acquired for all samples and fitted globally according to the FBM with Equations (S1) and (S2) in SI. The lifetime (τ_M) of the pyrene monomer was estimated by fitting the fluorescence decays of Py(2.3)-PLGA with a sum of exponentials. The low pyrene content of this sample ensured that it would form little excimer so that its long-lived behavior reflected isolated pyrenyl labels, whose decay time was attributed to τ_M . τ_M was found to decrease from 215 to 207 ns, when the GdHCl concentration was increased from zero to 0.1 M, before decreasing linearly with increasing GdHCl concentration from 207 to 190 ns from 0.1 and 5 M according to Equation (3). The lifetime τ_M was fixed in the fluorescence decay analysis to its value determined with Equation (3) for a given GdHCl concentration. This modest decrease in τ_M with increasing GdHCl concentration indicated that GdHCl is not an efficient quencher of pyrene.

$$\tau_M \text{ (ns)} = -3.33 \times [\text{GdHCl}] + 207 \quad (3)$$

The effect of GdHCl concentration on the monomer and excimer fluorescence decays can be seen in Figure 3, where the monomer and excimer fluorescence decays of Py(9.0)-PLGA are represented for GdHCl concentrations of 0.1, 1, and 5 M. The long-lived tails of the pyrene monomer decays in Figure 3A were essentially parallel, as expected since τ_M did not change much with GdHCl concentration. The early part of the monomer decay for Py(9.0)-PLGA in DMF with 0.1 M GdHCl showed a pronounced decrease reflecting efficient PEF, as would be expected if PLGA adopted a condensed conformation, such as that expected of an α -helix. This decrease in fluorescence intensity at the early times became less pronounced as more GdHCl was added to the solution, reflecting a decrease in PEF efficiency, that agreed with the I_E/I_M trends observed in Figure 2C. The decrease in PEF observed for the monomer decays as more GdHCl was added to the solution was also observed in the excimer decays in Figure 3B, that showed a longer rise time with increasing GdHCl concentration. Similar to the SSF spectra in Figure 1A, the fluorescence decays also indicated that the addition of GdHCl affected PEF, suggesting that these changes might be related to the conformational changes experienced by the PLGA α -helix in DMF.

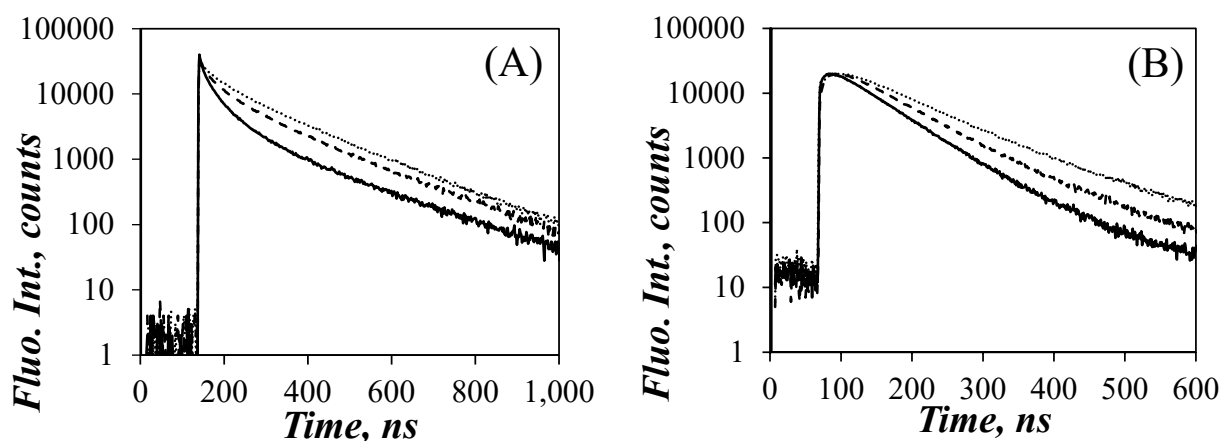


Figure 3. Fluorescence decays of the pyrene (A) monomer and (B) excimer of the Py(9.0)-PLGA solutions in DMF at different GdHCl concentrations. From bottom to top: $[GdHCl] = 0.1, 1.0, 5.0 \text{ mol}\cdot\text{L}^{-1}$ yielding N_{blob} values of 19, 15, and 11, respectively.

3.3. Fluorescence Blob Model Analysis of Decays

After determining the k_2 value at each GdHCl concentration, the k_2 value was fixed for a given GdHCl concentration and the fluorescence decays were fitted according to Equations (S1) and (S2). The N_{blob} values were determined by introducing the $\langle n \rangle$ values retrieved from the fluorescence decay analysis into Equation (1). The N_{blob} values obtained for the Py-PLGA and Py-PDLGA samples are plotted as a function of pyrene content for different GdHCl concentrations in Figure 4A,B, respectively. For each GdHCl concentration, and despite the scatter, the N_{blob} values clustered around a constant value indicating that the pyrene-labeling did not affect the behavior of the polymers. The main difference in behavior between the Py-PLGA and Py-PDLGA samples was that N_{blob} decreased continuously with increasing GdHCl concentration in Figure 4A while N_{blob} remained constant and equal to $10.4 (\pm 1.3)$ for the Py-PDLGA samples in Figure 4B. This effect was clearly illustrated in Figure 4C, where the N_{blob} values obtained as a function of pyrene content were averaged to yield $\langle N_{\text{blob}} \rangle$, which was plotted as a function of GdHCl concentration. $\langle N_{\text{blob}} \rangle$ decreased from $20.2 (\pm 1.8)$ for Py-PLGA in DMF without GdHCl to an average value of $10.2 (\pm 1.5)$ for Py-PLGA with 4 and 5 M GdHCl. An $\langle N_{\text{blob}} \rangle$ value of $20.2 (\pm 1.8)$ has been reported numerous times, when Py-PLGA adopts an α -helical conformation [9,10,12], as it is known to do in DMF [31]. With 4 and 5 M GdHCl, $\langle N_{\text{blob}} \rangle$ for Py-PLGA approached the $\langle N_{\text{blob}} \rangle$ value for randomly coiled Py-PDLGA in DMF, that remained constant and equal to $10.4 (\pm 1.3)$ at all GdHCl concentrations. Overall, the results in Figure 4C indicate that addition of GdHCl to a solution of α -helical PLGA in DMF induces the progressive unraveling of the PLGA α -helix, until it becomes a random coil at high GdHCl concentrations.

The FBM analysis of the fluorescence decays also yielded k_{blob} , which was plotted as a function of pyrene content in Figure 5A,B for the Py-PLGA and Py-PDLGA samples, respectively. In agreement with N_{blob} , k_{blob} did not change much with pyrene content within experimental error, again implying that the pyrene content did not affect the behavior of the polymers. The k_{blob} values obtained as a function of pyrene content in Figure 5A,B were averaged to yield $\langle k_{\text{blob}} \rangle$, which was plotted as a function of GdHCl concentration in Figure 5C. Within experimental error, the $\langle k_{\text{blob}} \rangle$ values for the Py-PLGA and Py-PDLGA samples showed a similar trend, with $\langle k_{\text{blob}} \rangle$ decreasing with increasing GdHCl concentration. The decrease in k_{blob} was most certainly a consequence of the increase in the solution viscosity associated with the addition of fairly large amounts of GdHCl and the main contributor to the decrease in the I_E/I_M ratios observed for the Py-PDLGAs in Figure 2D.

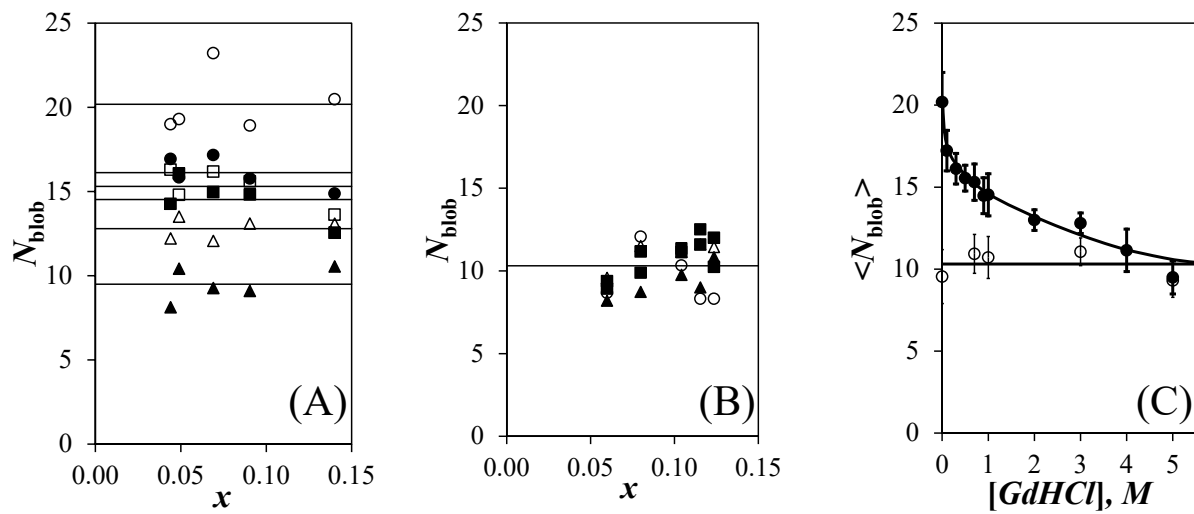


Figure 4. Plot of N_{blob} as a function of the mole fraction (x) of pyrene-labeled glutamic acids for (A) the Py-PLGA and (B) the Py-PDLGA samples in DMF with (○) 0 M, (●) 0.3 M, (□) 0.7 M, (■) 1 M, (△) 3 M, and (▲) 5 M GdHCl. (C) Plot of $\langle N_{\text{blob}} \rangle$ as a function of GdHCl concentration for (●) PLGA and (○) PDLGA.

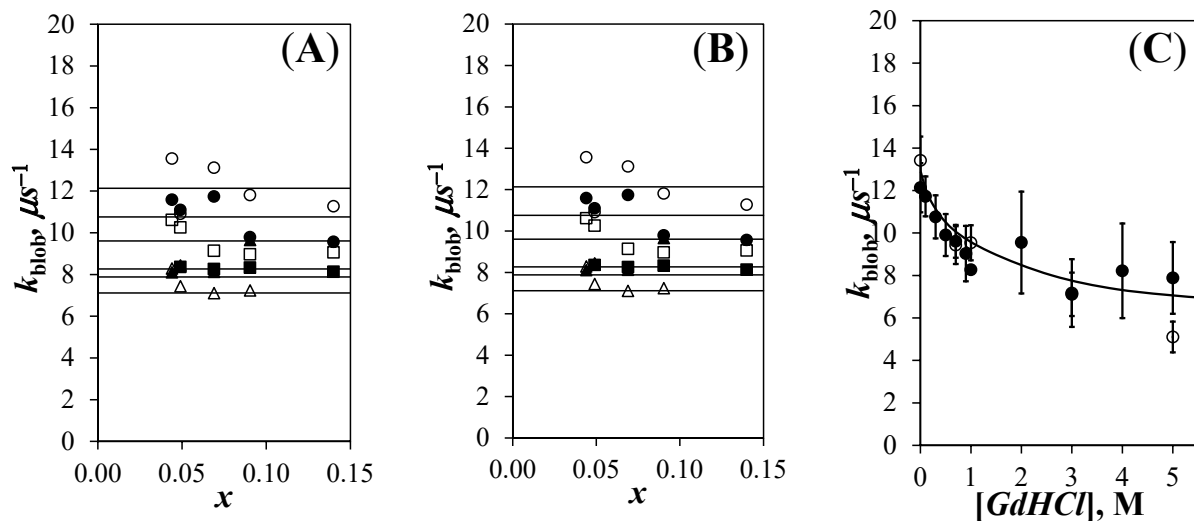


Figure 5. Plot of k_{blob} as a function of the mole fraction (x) of pyrene-labeled glutamic acids for (A) the Py-PLGA and (B) the Py-PDLGA samples in DMF with (○) 0 M, (●) 0.3 M, (□) 0.7 M, (■) 1 M, (△) 3 M, and (▲) 5 M GdHCl. (C) Plot of k_{blob} as a function of GdHCl concentration for (●) PLGA and (○) PDLGA.

The trends shown in Figures 4C and 5C displayed some remarkable features. A decrease in $\langle N_{\text{blob}} \rangle$, such as that displayed by the Py-PLGA samples in Figure 4C, is normally associated with smaller V_{blob} and larger $\langle k_{\text{blob}} \rangle$ values, since $k_{\text{blob}} = k_{\text{diff}} \times (1/V_{\text{blob}})$. The decrease of both $\langle N_{\text{blob}} \rangle$ in Figure 4C and $\langle k_{\text{blob}} \rangle$ in Figure 5C for the Py-PLGA samples with increasing GdHCl concentration was thus noticeable. The constancy of N_{blob} with GdHCl concentration found for the Py-PDLGA samples suggested that V_{blob} did not change. Therefore, the $\sim 30\%$ decrease in k_{blob} observed for Py-PDLGA must have been a consequence of the increase in viscosity associated with the addition of large amounts of GdHCl. The similarity of the $k_{\text{blob}}\text{-vs-}[\text{GdHCl}]$ trends in Figure 5C for both Py-PLGA and Py-PDLGA, coupled with the fact that they were labeled with pyrene in the same manner, suggested that both samples shared a same V_{blob} , which remained constant over the range of GdHCl concentrations studied. This implied that the decrease in N_{blob} found for Py-PLGA in Figure 4C with increasing GdHCl concentration reflected a decrease in the local polypeptide concentration experienced by an excited pyrenyl label, as expected with

the unravelling of the PLGA α -helix. The reduction in the local peptide concentration as Py-PLGA transitions from an α -helix to a random coil also leads to a reduction in $[Py]_{loc}$, which explains the more pronounced change in the I_E/I_M -vs-[GdHCl] trends observed for Py-PLGA than those observed for Py-PDLGA in Figure 2C,D, respectively.

In summary, N_{blob} appeared to be a direct measure of the number of structural units encompassed inside V_{blob} . Since V_{blob} did not change with GdHCl concentration, N_{blob} thus reflected the local density of the polypeptides in solution. This conclusion is supported by earlier reports, which also suggested that FBM experiments report directly on the local density of a polypeptide as experienced by an excited pyrenyl label [15,16]. Consequently, the results obtained up to this point suggested that the N_{blob} values reported in Figure 4C reflected the extent of structured PLGA existing in the solution, and could possibly be handled in the same manner as other structural parameters commonly used to gauge the structural content of polypeptides in solution such as ellipticity [20–25], fluorescence intensity [25,26], or fluorescence anisotropy [26]. The implication of this conclusion was that N_{blob} could be employed to probe the stability of a polypeptide upon addition of a denaturant. These considerations are discussed hereafter.

4. Discussion

4.1. Unfolding of a Protein According to the Two-State Model

The stability of a protein is usually defined by its ability to resist unfolding upon being subject to denaturing forces resulting from the addition of a denaturing agent, a sudden change in solution pH, or a step increase in temperature [28,29,34]. A quantitative measure of the stability of a protein is provided by the change in Gibbs energy ($\Delta_{unfold}G(H_2O)$) between the folded (N) and fully unfolded (D) conformation of a protein in water. Numerous reports in the literature suggest that the folding of many proteins follows the two-state model, whereby an equilibrium exists between the denatured and native state of proteins, as shown in Equation (4) [28,29].

$$\frac{K^{unfold}}{ND} \quad (4)$$

The equilibrium constant K^{unfold} describing the equilibrium between the native and unfolded protein can be related to $\Delta_{unfold}G(H_2O)$ according to Equation (5), where f_D and f_N represent the molar fractions of denatured and native protein, respectively. In turn, the ratio f_D/f_N is expected to be well represented by an experimental observable (Y), that accurately reflects the extent of denaturation experienced by the protein of interest.

$$K^{unfold} = \exp\left(-\frac{\Delta_{unfold}G(H_2O)}{RT}\right) = \frac{f_D}{f_N} = \frac{Y - Y_N}{Y_D - Y} \quad (5)$$

Based on the Linear Extrapolation Method (LEM) first introduced by Green and Pace [20], a plot of $\ln(f_D/f_N)$ should decrease linearly with the denaturant concentration as shown in Equation (6), with the y -intercept yielding $\Delta_{unfold}G(H_2O)$. In water, $\Delta_{unfold}G(H_2O)$ values around $\sim 40 \text{ kJ}\cdot\text{mol}^{-1}$ have been reported for ~ 300 aa-long proteins [29]. The slope (m) is related to the ability of the denaturant to unfold a protein and would take a value of $\sim 4 \text{ kJ}\cdot\text{mol}^{-1}\cdot\text{M}^{-1}$ [29].

$$-\ln(f_D/f_N) = \Delta_{unfold}G(DMF) - m \times [GdHCl] \quad (6)$$

4.2. Using $\langle N_{blob} \rangle$ as a Structural Parameter

Since the $\langle N_{blob} \rangle$ -vs-[GdHCl] trends obtained in Figure 4C suggested that $\langle N_{blob} \rangle$ reflected the structural content of the Py-PLGA samples in DMF as a function of GdHCl concentration, we decided to investigate whether $\langle N_{blob} \rangle$ could be taken as such an observable (i.e., $Y = \langle N_{blob} \rangle$ in Equation (5)) to determine $\Delta_{unfold}G(DMF)$ for the unfolding of an α -helical PLGA in DMF into a random coil upon addition of GdHCl. We also note that while the ellipticity of a protein determined by circular dichroism is normally the

observable of choice to determine $\Delta_{\text{unfold}}G(\text{H}_2\text{O})$, the strong amide absorption of DMF would rule out the use of CD to determine $\Delta_{\text{unfold}}G(\text{DMF})$ for the unfolding of a protein in DMF. The $\langle N_{\text{blob}} \rangle$ values obtained in Figure 4C were introduced into Equation (5) to determine the $f_{\text{D}}/f_{\text{N}}$ ratio for GdHCl concentrations between 0.3 and 2 M, using an $\langle N_{\text{blob}} \rangle$ value of 20.2 and 10.4 obtained for α -helical Py-PLGA in DMF without GdHCl and randomly coiled Py-PDLGA in DMF over all GdHCl concentrations for the Y_{N} and Y_{D} values, respectively. $-\ln(f_{\text{D}}/f_{\text{N}})$ was plotted as a function of GdHCl concentration in Figure 6. A satisfactory straight line was obtained with an intercept corresponding to a $\Delta_{\text{unfold}}G(\text{DMF})$ value of $1.3 (\pm 0.2) \text{ kJ}\cdot\text{mol}^{-1}$ and an m value of $1.9 (\pm 0.2) \text{ kJ}\cdot\text{mol}^{-1}\cdot\text{M}^{-1}$.

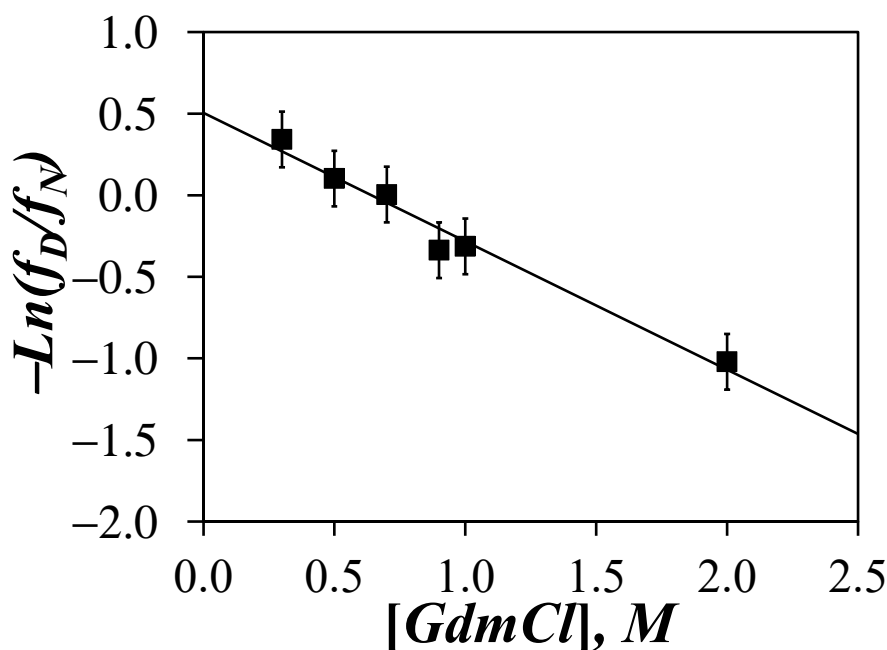


Figure 6. Plot of $-\ln(f_{\text{D}}/f_{\text{N}})$ as a function of GdHCl concentration where f_{D} and f_{N} are calculated from the $\langle N_{\text{blob}} \rangle$ values obtained for Py-PLGA trend shown in Figure 4C.

Application of the LEM using $\langle N_{\text{blob}} \rangle$ as an experimental observable to measure $\Delta_{\text{unfold}}G(\text{DMF})$ for the unfolding of PLGA in DMF upon the addition of GdHCl resulted in a surprisingly good linearity between $-\ln(f_{\text{D}}/f_{\text{N}})$ and the GdHCl concentration in Figure 6. The $\Delta_{\text{unfold}}G(\text{DMF})$ value of $1.3 (\pm 0.2) \text{ kJ}\cdot\text{mol}^{-1}$ obtained from the y -intercept of the plot was more than one order of magnitude lower than the $\Delta_{\text{unfold}}G(\text{H}_2\text{O})$ values reported for the unfolding of globular proteins in water [29]. Such a difference between $\Delta_{\text{unfold}}G(\text{DMF})$ and $\Delta_{\text{unfold}}G(\text{H}_2\text{O})$ was to be expected. Beside the fact that DMF was used instead of H_2O , the main difference in stability between PLGA and proteins was most likely due to the extended conformation of α -helical PLGA, which could not benefit from the many additional stabilizing interactions existing between the structural motives found in the interior of globular proteins in water [35–38]. Instead, internal H-bonds between the amide bonds of the polypeptide backbone were the only stabilizing contributions to the structural integrity of the PLGA α -helix [39], which were easily neutralized by the addition of GdHCl. These considerations rationalize the rather low $\Delta_{\text{unfold}}G(\text{DMF})$ value obtain for PLGA in DMF. Although low, the m value of $1.9 (\pm 0.2) \text{ kJ}\cdot\text{mol}^{-1}\cdot\text{M}^{-1}$ retrieved for PLGA was only half the value expected for globular proteins, suggesting that the unfolding of the PLGA α -helix in DMF results in substantial exposure of the glutamic acid residues to the solvent.

4.3. Strengths and Weaknesses of PEF-Based Macromolecular Structure Determination

As already discussed in earlier works [7–12], the FBM analysis of the PEF signal generated by macromolecules randomly labeled with pyrene yields the parameter N_{blob} ,

which describes the conformation of structured macromolecules in solution. The fact that the macromolecule needs to be randomly labeled does not require specific attachment points, and can be polydisperse represents important advantages to the method. It also takes advantage of the outstanding sensitivity of fluorescence to probe macromolecules under extremely dilute conditions, typically at concentrations around 1 mg/L, two-to-three orders of magnitude lower than most other standard techniques used for structure determination like scattering or NMR. Despite its formidable advantages, the PEF-based method also has some important disadvantages, which should not be overlooked. First, pyrene is hydrophobic and aggregates in water, making the structural study of pyrene-labeled macromolecules in water challenging [40]. Second, the random labeling of a macromolecule is well suited to characterize its structure in solution as long as the pyrenyl labels are attached at its periphery such as onto the side groups of helices of amylose [7] or PLGA or poly(L-lysine) [8–12]. In the case of a protein containing several closely packed structural motives, the random introduction of pyrenyl labels onto the motives would interfere with their tight packing, which would affect the structure of the protein. Third, a PEF experiment reports on a macromolecular structure over a length scale, that is defined by the reach of a pyrenyl label bound to the macromolecule via a linker of specific length. In the case of the PGAs randomly labeled with 1-pyrenemethylamine, the maximum distance separating two α -carbon in the polypeptide backbone would equal 3.1 (± 0.2) and 3.1 (± 0.4) nm for α -helical PLGA and randomly coiled PDLGA constructs, which corresponded to $\langle N_{\text{blob}} \rangle$ values of 20.5 (± 1.5) and 10.5 (± 1.5) in DMF, respectively. Fourth, polymers containing chemical groups such as amines [11] or primary amides (but not secondary or tertiary amides) capable of quenching the pyrene fluorescence cannot be studied. Nevertheless, and despite these drawbacks, many synthetic and natural polymers remain, whose characterization would strongly benefit from the determination of their conformation in solution through a PEF study.

5. Conclusions

A series of experiments were conducted, where the PEF of Py-PLGA and Py-PDLGA constructs in DMF was analyzed with the FBM to yield $\langle N_{\text{blob}} \rangle$ as a function of the amount of GdHCl, a known denaturing agent [27], that was added to the solution. $\langle N_{\text{blob}} \rangle$ decreased progressively from a value of 20.2 (± 1.8) for Py-PLGA in DMF without GdHCl to 10.2 (± 1.5) in DMF with 4 or 5 M GdHCl. Since $\langle N_{\text{blob}} \rangle$ values of ~ 20 and ~ 10 are those expected for α -helical and randomly coiled Py-PLGA, respectively [9,10,12], the $\langle N_{\text{blob}} \rangle$ -*vs*-[GdHCl] trend obtained for Py-PLGA in Figure 4C was taken as evidence that these FBM experiments reflected the unravelling of the PLGA α -helix as GdHCl was added to the solution. Furthermore, the constancy of $\langle N_{\text{blob}} \rangle$ observed for the Py-PDLGA samples suggested that the *blob* volume (V_{blob}) remained constant with GdHCl concentration and that the decrease in k_{blob} with increasing GdHCl concentration observed for Py-PDLGA must have been due to an increase in solution viscosity with increasing GdHCl concentration. Combining the constancy in V_{blob} with the similarity of the k_{blob} -*vs*-[GdHCl] plots obtained for the Py-PLGA and Py-PDLGA samples led to the conclusion, that V_{blobs} remained constant for the Py-PLGA samples and that N_{blob} reflected the change in polymer density experienced by an excited pyrenyl label as the PLGA α -helix unraveled upon addition of GdHCl. This conclusion agreed with those reached in earlier studies [15,16] and represents an important improvement in the applicability of the FBM to probe the local density of macromolecules in solution, a feature that used to be mainly accessible by scattering techniques.

The inferred ability of $\langle N_{\text{blob}} \rangle$ to report on the extent of structural content of the PLGA α -helix was further confirmed by applying the LEM to determine the change in Gibbs energy ($\Delta_{\text{unfold}}G(\text{DMF})$) for the unfolding of PLGA in DMF upon addition of GdHCl. The good linearity observed in Figure 6 between $-Ln(f_{\text{D}}/f_{\text{N}})$ and the GdHCl concentration suggested that $\langle N_{\text{blob}} \rangle$ reported accurately on the structural content of PLGA. The low $\Delta_{\text{unfold}}G(\text{DMF})$ value retrieved from this analysis was mostly a consequence of dealing with

an isolated α -helix, whose stability was the result of intramolecular H-bonding between the backbone amides [39]. These would represent fairly weak interactions compared to those experienced by the different structural motives inside a globular proteins [35–38], which must contribute to the higher $\Delta_{\text{unfold}}G(\text{H}_2\text{O})$ values obtained for the unfolding of proteins in aqueous solutions.

In summary, this study provides further support to the notion that a combination of PEF and FBM analysis of pyrene-labeled macromolecules yields information about the density of macromolecules in solution. Because PEF occurs locally over ~ 3 nm in the case of Py-PGA constructs, the ability to use N_{blob} to probe the density of macromolecules over a ~ 3 nm length scale offers a means to probe macromolecules in solution at close range, a feature that should nicely complement the studies of macromolecules by scattering techniques, that typically probe entire macromolecules. Consequently, the PEF study of pyrene-labeled macromolecules opens new venues of research to characterize the conformation of complex macromolecules in solution.

Supplementary Materials: The following are available online at <https://www.mdpi.com/article/10.3390/polym13111690/s1>, FBM equations, plot of k_2 as a function of GdHCl concentration, tables of parameters retrieved from the FBM of the fluorescence decays acquired with the Py-PLGA and Py-PDLGA samples.

Author Contributions: W.Y. conducted all experiments and wrote the first draft of this manuscript; R.C. ensured the day-to-day supervision and training of W.Y. and prepared the polypeptides used in this study; J.D. oversaw the project and wrote the final report submitted for publication. All authors have read and agreed to the published version of the manuscript.

Funding: This research was funded by the Natural Sciences and Engineering Research Council of Canada (NSERC).

Institutional Review Board Statement: Not applicable.

Informed Consent Statement: Not applicable.

Data Availability Statement: The data presented in this study are available on request from the corresponding author.

Conflicts of Interest: The authors declare no conflict of interest. The funders had no role in the design of the study; in the collection, analyses, or interpretation of data; in the writing of the manuscript, or in the decision to publish the results.

References

1. Mathew, A.; Siu, H.; Duhamel, J. A Blob Model to Study Chain Folding by Fluorescence. *Macromolecules* **1999**, *32*, 7100–7108. [[CrossRef](#)]
2. Duhamel, J. Polymer Chain Dynamics in Solution Probed with a Fluorescence Blob Model. *Acc. Chem. Res.* **2006**, *39*, 953–960. [[CrossRef](#)] [[PubMed](#)]
3. Duhamel, J. New Insights in the Study of Pyrene Excimer Fluorescence to Characterize Macromolecules and their Supramolecular Assemblies in Solution. *Langmuir* **2012**, *28*, 6527–6538. [[CrossRef](#)] [[PubMed](#)]
4. Duhamel, J. Global Analysis of Fluorescence Decays to Probe the Internal Dynamics of Fluorescently Labeled Macromolecules. *Langmuir* **2014**, *30*, 2307–2324. [[CrossRef](#)] [[PubMed](#)]
5. Farhangi, S.; Duhamel, J. Long Range Polymer Chain Dynamics Studied by Fluorescence Quenching. *Macromolecules* **2016**, *49*, 6149–6162. [[CrossRef](#)]
6. Hall, T.; Whitton, G.; Casier, R.; Gauthier, M.; Duhamel, J. Arborescent Poly(L-glutamic acid)s as Standards to Study the Dense Interior of Polypeptide Mesoglobules by Pyrene Excimer Fluorescence. *Macromolecules* **2018**, *51*, 7914–7923. [[CrossRef](#)]
7. Li, L.; Duhamel, J. Conformation of Pyrene-Labeled Amylose in DMSO Characterized with the Fluorescence Blob Model. *Macromolecules* **2016**, *49*, 7965–7974. [[CrossRef](#)]
8. Duhamel, J.; Kanagalingam, S.; O'Brien, T.; Ingratta, M. Side-Chain Dynamics of an α -Helical Polypeptide Monitored by Fluorescence. *J. Am. Chem. Soc.* **2003**, *125*, 12810–12822. [[CrossRef](#)]
9. Ingratta, M.; Duhamel, J. Effect of Side-chain Length on the Side-chain Dynamics of α -Helical Poly(L-glutamic acid) as Probed by a Fluorescence Blob Model. *J. Phys. Chem. B* **2008**, *112*, 9209–9218. [[CrossRef](#)] [[PubMed](#)]
10. Casier, R.; Duhamel, J. Pyrene Excimer Fluorescence as a Direct and Easy Experimental Means to Characterize the Length Scale and Dynamics of Polypeptide Foldons. *Macromolecules* **2018**, *51*, 3450–3457. [[CrossRef](#)]

11. Casier, R.; Duhamel, J. The Effect of Structure on Polypeptide Blobs: A Model Study Using Poly(L-Lysine). *Langmuir* **2020**, *36*, 7980–7990. [[CrossRef](#)] [[PubMed](#)]
12. Casier, R.; Duhamel, J. The Effect of Like-Charges on the Conformation and Internal Dynamics of Polypeptides Probed by Pyrene Excimer Fluorescence. *Macromolecules* **2020**, *53*, 5147–5157. [[CrossRef](#)]
13. Li, L.; Kim, D.; Zhai, X.; Duhamel, J. A Pyrene Excimer Fluorescence (PEF) Study of the Interior of Amylopectin in Dilute Solution. *Macromolecules* **2020**, *53*, 6850–6860. [[CrossRef](#)]
14. Li, L.; Duhamel, J. Interior of Amylopectin and Nanosized Amylopectin Fragments Probed by Viscometry, Dynamic Light Scattering, and Pyrene Excimer Formation. *Polymers* **2020**, *12*, 2649. [[CrossRef](#)] [[PubMed](#)]
15. Casier, R.; Duhamel, J. Blob-Based Approach to Estimate the Folding Time of Proteins Supported by Pyrene Excimer Fluorescence Experiments. *Macromolecules* **2020**, *53*, 9823–9835. [[CrossRef](#)]
16. Casier, R.; Duhamel, J. Blob-Based Predictions of Protein Folding Times from the Amino Acid Dependent Conformation of Polypeptides in Solution. *Macromolecules* **2021**, *54*, 919–929. [[CrossRef](#)]
17. Schatz, C.; Pichot, C.; Delair, T.; Viton, C.; Domard, A. Static Light Scattering Studies on Chitosan Solutions: From Macromolecular Chains to Colloidal Dispersions. *Langmuir* **2003**, *19*, 9896–9903. [[CrossRef](#)]
18. Rajapaksha, A.; Stanley, C.B.; Todd, B.A. Effects of Macromolecular Crowding on the Structure of a Protein Complex: A Small Angle Scattering Study of Peroxide Dismutase. *Biophys. J.* **2015**, *108*, 967–974. [[CrossRef](#)]
19. Kikuchi, M.; Nakano, R.; Jinbo, Y.; Saito, Y.; Ohno, S.; Togashi, D.; Enomoto, K.; Narumi, A.; Haba, O.; Kawaguchi, S. Graft Density Dependence of Main Chain Stiffness in Molecular Rod Brushes. *Macromolecules* **2015**, *48*, 5878–5886. [[CrossRef](#)]
20. Greene, R.F.; Pace, C.N. Urea and Guanidinium Hydrochloride Denaturation of Ribonuclease, Lysozyme, α -Chymotrypsin, and b-Lactoglobulin. *J. Biol. Chem.* **1974**, *249*, 5388–5393. [[CrossRef](#)]
21. Santoro, M.M.; Bolen, D.W. Unfolding Free Energy Changes Determined by the Linear Extrapolation Method. 1. Unfolding of Phenylmethanesulfonyl α -Chymotrypsin Using Different Denaturants. *Biochemistry* **1988**, *27*, 8063–8068. [[CrossRef](#)]
22. Santoro, M.M.; Bolen, D.W. A Test of the Linear Extrapolation of Unfolding Free Energy Changes over an Extended Denaturant Concentration Range. *Biochemistry* **1992**, *31*, 4901–4907. [[CrossRef](#)]
23. Smith, J.S.; Scholtz, J.M. Guanidine Hydrochloride Unfolding of Peptide Helices: Separation of Denaturant and Salt Effects. *Biochemistry* **1996**, *35*, 7292–7297. [[CrossRef](#)]
24. Curnow, P.; Booth, P.J. Combined Kinetic and Thermodynamic Analysis of α -Helical Membrane Protein Unfolding. *Proc. Natl. Acad. Sci. USA* **2007**, *104*, 18970–18975. [[CrossRef](#)]
25. Findlay, H.E.; Rutherford, N.G.; Henderson, P.J.F.; Booth, P.J. Unfolding Free Energy of a Two Domain Transmembrane Sugar Transport Protein. *Proc. Natl. Acad. Sci. USA* **2010**, *107*, 18451–18456. [[CrossRef](#)]
26. Patra, M.; Mukhopadhyay, C.; Chakrabarti, A. Probing Conformational Stability and Dynamics of Erythroid and Nonerythroid Spectrin: Effect of Urea and Guanidine Hydrochloride. *PLoS ONE* **2015**, *10*, e0116991. [[CrossRef](#)]
27. Tanford, C.; Kawahara, K.; Lapanje, S. Proteins as Random Coils. I. Intrinsic Viscosity and Sedimentation Coefficients in Concentrated Guanidine Hydrochloride. *J. Am. Chem. Soc.* **1967**, *89*, 729–736. [[CrossRef](#)]
28. Flecha, F.L.G. Kinetic Stability of Membrane Proteins. *Biophys. Rev.* **2017**, *9*, 563–572. [[CrossRef](#)]
29. Kazlauskas, R. Engineering more Stable Proteins. *Chem. Soc. Rev.* **2018**, *47*, 9026–9045. [[CrossRef](#)]
30. Press, W.H.; Flannery, B.P.; Teukolsky, S.A.; Vetterling, W.T. *Numerical Recipes. The Art of Scientific Computing (Fortran Version)*; Cambridge University Press: Cambridge, UK, 1992; p. 82.
31. Yamaoka, K.; Ueda, K. Reversing-Pulse Electric Birefringence Study of Helical Poly(α -L-glutamic acid) in *N,N*-Dimethylformamide with Emphasis on a New Data Analysis for the Polydisperse System. *J. Phys. Chem.* **1982**, *86*, 406–413. [[CrossRef](#)]
32. Cuniberti, C.; Perico, A. Intramolecular Excimer Formation in Polymers. Pyrene-Labeled Polyvinylacetate. *Eur. Polym. J.* **1980**, *16*, 887–893. [[CrossRef](#)]
33. Lakowicz, J.R. *Principles of Fluorescence Spectroscopy*, 2nd ed.; Kluwer Acad.: New York, NY, USA, 1999; p. 241.
34. Bedouelle, P. Principles and Equations for Measuring and Interpreting Protein Stability: From Monomer to Tetramer. *Biochimie* **2016**, *121*, 29–37. [[CrossRef](#)]
35. Karshikoff, A.; Ladenstein, R. Ion Pairs and the Thermotolerance of Proteins from Hyperthermophiles: A ‘Traffic Rule’ for Hot Roads. *Trends Biochem. Sci.* **2001**, *26*, 550–557. [[CrossRef](#)]
36. Kumar, S.; Nussinov, R. Close-Range Electrostatic Interactions in Proteins. *ChemBioChem* **2002**, *3*, 604–617. [[CrossRef](#)]
37. Fass, D. Disulfide Bonding in Protein Biophysics. *Annu. Rev. Biophys.* **2012**, *41*, 63–79. [[CrossRef](#)]
38. Pace, N.C.; Scholtz, J.M.; Grimsley, G.R. Forces Stabilizing Proteins. *FEBS Lett.* **2014**, *588*, 2177–2184. [[CrossRef](#)]
39. Pauling, L.; Corey, R.B.; Branson, H.R. The Structure of Proteins: Two Hydrogen-Bonded Helical Configurations of the Polypeptide Chain. *Proc. Natl. Acad. Sci. USA* **1951**, *37*, 205–211. [[CrossRef](#)]
40. Winnik, F.M.; Winnik, F.M. Photophysics of Preassociated Pyrenes in Aqueous Polymer Solutions and in Other Organized Media. *Chem. Rev.* **1993**, *93*, 587–614. [[CrossRef](#)]